Article

Observation of a Polarization-Assisted Dipole-Bound State

Dao-Fu Yuan, Yuan Liu, Yue-Rou Zhang, and Lai-Sheng Wang*

ACCESS | Metrics & More | Article Recommendations | SI Supporting Information

ABSTRACT: The critical dipole moment to bind an electron was empirically determined to be 2.5 debye, even though smaller values were predicted theoretically. Herein, we report the first observation of a polarization-assisted dipole-bound state (DBS) for a molecule with a dipole moment below 2.5 debye. Photoelectron and photodetachment spectroscopies are conducted for cryogenically cooled indolide anions, where the neutral indolyl radical has a dipole moment of 2.4 debye. The photodetachment experiment reveals a DBS only 6 cm^{-1} below the detachment threshold along with sharp vibrational Feshbach resonances. Rotational profiles are observed for all of the Feshbach resonances, which are found to have surprisingly narrow linewidths and long autodetachment

Long-Lived Polarization-Assisted Dipole-Bound State

lifetimes attributed to weak coupling between vibrational motions and the nearly free dipole-bound electron. Calculations suggest that the observed DBS has π-symmetry stabilized by the strong anisotropic polarizability of indolyl.
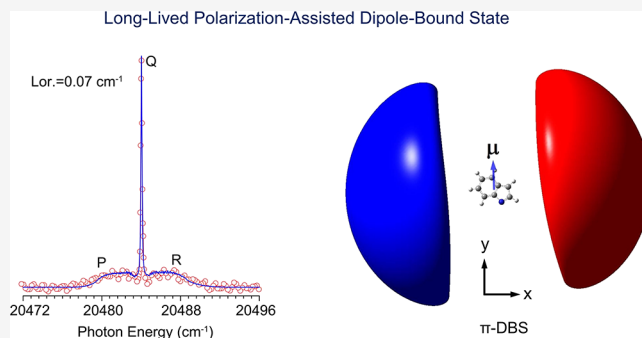
1. INTRODUCTION

Fermi and Teller first suggested that a stationary dipole with a dipole moment larger than 1.625 debye can bind an electron.[1] Few decades later, this critical dipole moment for electron binding was rediscovered by many researchers, as succinctly discussed by Turner.[2] For real molecular systems, the critical dipole moment for electron binding was predicted to be ~2 debye, when non-Born–Oppenheimer effects were considered.[3−7] Molecules are many-body systems, for which correlation and polarization effects also play important roles in the binding of the dipole-bound electron.[8−10] Experimentally, the minimum dipole moment to form a dipole-bound anion was empirically determined to be 2.5 debye.[11−14] No molecules with a dipole moment less than 2.5 debye have been observed to form dipole-bound anions. Stable valence-bound anions can support dipole-bound states (DBSs) as electronically excited states just below the electron detachment threshold,[15−19] analogous to Rydberg states of neutral molecules. To minimize molecule-dependent effects, a series of halogen-substituted phenoxide anions with a similar structure and size but different dipole moments were studied, and the binding energies of their excited DBS were also extrapolated to a critical dipole moment of 2.5 debye at zero binding energy.[20]

The formation of DBS or dipole-bound anions is not only of fundamental interest but is also important in many chemical and physical processes. DBSs have been suggested as the "doorway" states before an electron is captured to form a stable valence-bound anion both in biological systems and in the interstellar medium.[21−26] Anions that can support DBSs have been hypothesized to be potential carriers for the enigmatic

diffuse interstellar bands.[27−31] Many experimental methods have been used to study DBSs.[11−22,30−40] A key advance in the past few years in the study of DBS has been the coupling of an electrospray ion source with a three-dimensional (3D) cryogenic Paul trap to create cold anions[41−44] that have enabled high-resolution photodetachment and resonant photo-electron spectroscopy (PES) and allowed the precise measurements of the binding energies of excited DBSs.[45−50] It has also made it possible recently for pump–probe experiments that can directly investigate the vibrational autodetachment dynamics of DBSs.[51−53]

Herein, we report the observation of a polarization-assisted DBS for a molecular system with a dipole moment less than 2.5 debye for the first time. Photodetachment spectroscopy of cryogenically cooled indolide anions ($C_8NH_6^-$, Scheme 1) reveals a DBS only 6 cm^{-1} below the detachment threshold and 17 above-threshold vibrational peaks (Feshbach resonances), even though the dipole moment of the indolyl radical core ($C_8NH_6^\bullet$) is only 2.4 debye. Theoretical calculations suggest that the observed excited DBS is of π-symmetry stabilized by the anisotropic polarizability of the delocalized π electrons of the aromatic rings in indolyl. All of the Feshbach resonances are observed to be surprisingly sharp with clearly
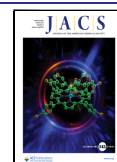
Scheme 1. Structure of the Indolide Anion[a]
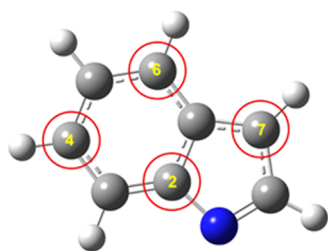
[a]The four carbon atoms with the appended diffuse bases are circled and labeled with numbers.

resolved rotational profiles, suggesting long autodetachment lifetimes.

2. EXPERIMENTAL AND THEORETICAL METHODS

2.1. Experimental Details. The experiments were carried out using our third-generation electrospray ionization−photoelectron spectroscopy (ESI-PES) apparatus.[42] The indolide anions were produced by electrospray of a 1 mM solution of indole (Sigma-Aldrich, ≥97%) in a mixed solvent of CH_3OH/H_2O (9/1 in volume) at a pH value of ∼10. Anions generated in the ESI source were guided into a cryogenically cooled 3D Paul trap operated at 4.6 K.[41,42] After being accumulated for 0.1 s and thermally cooled via collisions with a 1 mTorr mixed background gas (He/H_2: 4:1 in volume),[41] the anions were pulsed out at a 10 Hz repetition rate into the extraction zone of a time-of-flight mass spectrometer. The indolide anions due to deprotonation of indole were selected by a mass gate and photodetached in the interaction zone of the imaging lens by the fundamental output or second harmonic of a tunable dye laser. Photoelectrons were projected onto a pair of 75 mm diameter microchannel plates coupled to a phosphor screen and captured by a charge-coupled-device camera. The PE images were inverse-Abel transformed and reconstructed using the programs pBasex[54] and BASEX.[55] The PE spectra were calibrated with the known spectra of Au⁻ at different photon energies. The kinetic energy (KE) resolution was 3.8 cm⁻¹ for electrons with 55 cm⁻¹ KE and about 1.5% (ΔKE/KE) for KE above 1 eV in the current experiment.[42] Photodetachment spectra were obtained by measuring the total electron yield as a function of photon energies. Different scan steps were used and the finest scan step was 0.001 nm/step.

2.2. Franck−Condon and Rotational Simulations. The Franck−Condon (FC) factors from the anion ground state to vibrational levels of the neutral were calculated using FC-LAB2[56] with the optimized geometries and computed vibrational frequencies (scaled by a factor of 0.98) by density functional theory (DFT) at the B3LYP/aug-cc-pVTZ level of theory. The DFT calculations were performed using the Gaussian 09 package.[57]

The rotational profiles of vibrational transitions in the photo-detachment spectra were simulated using the PGOPHER program[58] with the calculated rotational constants for indolide (a = 3953.66 MHz, b = 1674.94 MHz, c = 1176.69 MHz) and indolyl (a = 3992.94 MHz, b = 1671.94 MHz, c = 1178.48 MHz). Both indolide and indolyl with C_s symmetry can be viewed as near-prolate symmetric tops (with the rotational inertia $I_A < I_B \sim I_C$) with the top axis (a-axis) and b-axis lying inside the molecular plane and the c-axis being perpendicular to the molecular plane. Under C_s symmetry, vibrational transitions to in-plane modes (A′) should give c-type rotational profiles while those to out-of-plane modes (A″) should yield b-type rotational profiles.[59] The linewidth of the excitation laser (0.08 cm⁻¹) was considered as Gaussian broadening. The rotational transitions were fitted as Lorentz line shape (lifetime broadening). The simulation yielded T_{rot} of ∼30 K.

2.3. Electronic Structure Calculations. Geometry optimizations and calculations of the ground-state electronic structure and rotational constants were performed using DFT at the B3LYP/aug-cc-pVTZ

level of theory. The first vertical detachment energy (VDE) was computed as the energy difference between the neutral and the anion at the anion geometry. The VDEs for excited states were obtained using time-dependent DFT (TD-DFT) with the same functional and basis set as the ground state calculation. The electronic structure calculations were followed by vibrational, electrostatic, and polarizability analyses. All of the calculated vibrational frequencies were scaled by a factor of 0.98 for comparison with the experimental measurements (Tables S1 and S2 in the Supporting Information). All electronic structure calculations were performed using the Gaussian 09 package.[57] The optimized neutral indolide geometry was used to perform TD-DFT calculations at the CAM-B3LYP/Def2-TZVPP +4s3p2d1f level of theory to search for weakly bound excited states of the anion near the detachment threshold. Diffuse bases were appended to four carbon atoms as labeled in Scheme 1. The exponents of the diffuse bases used were 4s (0.03942165641, 0.01633033298, 0.00676480391, 2.80230488E-3), 3p (0.03501152294, 0.01218880611, 4.2433742354E-3), 2d (0.0921823154, 2.6721947401E-2), 1f (0.25366666667). The binding energies for the two lowest excited states of the anion with their symmetries and electronic configurations were calculated.

3. RESULTS

3.1. Electron Affinity and Electronic Structure of Neutral Indolyl. Figure 1 shows the PE image and spectrum
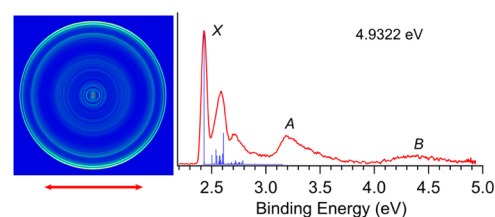

Figure 1. PE image and spectrum of indolide at 4.9322 eV. The FC factors are included as blue sticks for comparison. The double arrow below the image represents the polarization direction of the detachment laser.

of indolide at 4.9322 eV (39781 cm⁻¹). Three PES bands are observed, X, A, and B, due to detachment from the highest occupied molecular orbital (HOMO), HOMO-1, and HOMO-2 of indolide, respectively (Figure S1 in the Supporting Information). The observed vibrational profile of band X is consistent with the computed FC factors (Figure 1) and two previous PES studies.[60,61] Bands X, A, and B are measured to be at 2.43, ∼3.2, and ∼4.3 eV, respectively, in good agreement with the DFT and TD-DFT calculations (Table S3).

High-resolution photoelectron spectra are obtained for band X at lower photon energies, as shown in Figure 2. The electron affinity (EA) of the indolyl radical is measured accurately as 2.4311 ± 0.0004 eV (19,608 ± 3 cm⁻¹) in the near-threshold spectrum at 2.4346 eV, consistent with previous reports: 2.4315 ± 0.0017 eV from ref 60 and 2.430 ± 0.001 eV from ref 62. Numerous vibrational fine features (A to N) are resolved in the 2.5300 and 2.6206 eV spectra (Figure 2). The comparison between the experimental nonresonant spectrum at 2.6206 eV and the calculated FC factors is shown in Figure S2. The binding energies of all of the observed vibrational peaks are summarized in Table 1, along with the spectral assignments (vide infra) and theoretical values.

3.2. Searching for the DBS of Indolide and Resonant PES. The indolyl radical has a dipole moment of 2.4 debye (Table S4), which is slightly below the empirical critical dipole
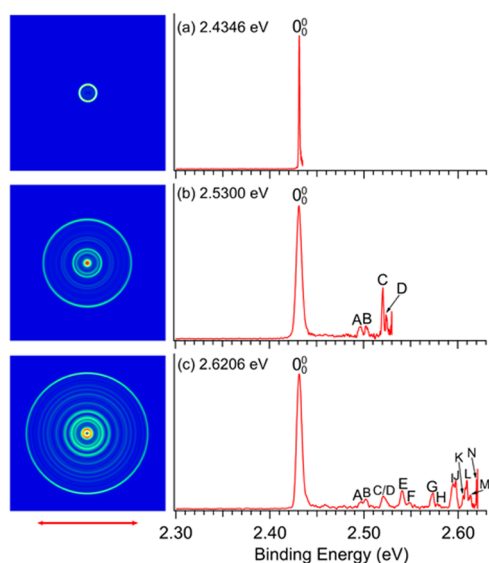
Journal of the American Chemical Society
pubs.acs.org/JACS
Article

Figure 2. Nonresonant PE images and spectra of indolide at (a) 2.4346 eV, (b) 2.5300 eV, and (c) 2.6206 eV. Peak 0_0^0 represents the 0−0 detachment transition. Peaks A−N denote transitions to different vibrational levels of indolyl. The double arrow below the image represents the polarization direction of the detachment laser.

Table 1. Assignments of the Observed Peaks in the Nonresonant and Resonant PE Spectra (*vide infra*)[a]

peak	binding energy (eV)[b]	binding energy (cm^{-1})[b]	shift (cm^{-1})	assignments	calculations (cm^{-1})[c]
0_0^0	2.4311(4)	19,608(3)			
A	2.4963(6)	20,134(5)	526	$36^1/26^1$	532/534
B	2.5020(10)	20,180(8)	572	$25^1/35^1$	575/564
C	2.5203(5)	20,328(4)	720	$34^1/39^136^1$	729/730
D	2.5246(8)	20,362(6)	754	24^1	755
E	2.5407(10)	20,492(8)	884	22^1	881
F	2.5478(10)	20,549(8)	941	$21^1/29^1$	947/944
G	2.5726(6)	20,749(5)	1141	$18^1/17^1$	1139/1146
H	2.5776(12)	20,790(10)	1182	16^1	1178
I	2.5944(6)	20,925(5)	1317	13^1	1319
J	2.5978(6)	20,953(5)	1345	12^1	1346
K	2.6049(5)	21,010(4)	1402	27^120^1	1405
L	2.6088(9)	21,041(7)	1433	$10^1/11^1$	1437/1431
M	2.6132(7)	21,077(6)	1469	9^1	1465
N	2.6197(5)	21,129(4)	1521	25^121^1	1522
a	2.4550(20)	19,801(16)	193	39^1	198
b	2.4808(12)	20,009(10)	401	$27^1/37^1$	400/404
c	2.5351(8)	20,447(6)	839	23^1	837
d	2.5556(12)	20,612(10)	1004	20^1	1005
e	2.5646(6)	20,685(5)	1077	19^1	1074
f	2.5811(8)	20,818(6)	1210	15^1	1208
g	2.5854(10)	20,853(8)	1245	34^126^1	1263
h	2.5891(7)	20,882(6)	1274	$14^1/36^124^1$	1277/1287

[a]The peaks labeled with lowercase letters are new features from the resonant PE spectra. [b]Numbers in the parentheses indicate the experimental uncertainties in the last digit. [c]Calculated frequencies are scaled by 0.98.

moment (2.5 debye) to support a DBS.[20] A previous photodetachment study of indolide revealed a strong threshold peak, which was suggested as possible evidence of a DBS with a low binding energy, but no vibrational Feshbach resonances were observed.[62] When we first conducted the photodetach-

ment experiment with a laser scan rate of 0.1 nm/step, we also observed a threshold enhancement but did not observe any DBS features expected as sharp resonances in the otherwise continuous electron signals. Much to our surprise, when we used a 0.005 nm/step scan rate, we discovered extraordinarily sharp resonances in the photodetachment spectrum, as shown in Figure 3. In a photon energy range up to 21,150 cm^{-1} (2.6223 eV), we observed seventeen vibrational Feshbach resonances (peaks 1−17), in addition to the bound zero-point level (peak 0).

Using the finest scan step available with our dye laser (0.001 nm/step), we are able to resolve rotational fine features for each Feshbach resonance. The rotational profile for the zero-point level is shown in Figure 3b, and the rotational profile for the Feshbach resonances 2, 3, and 5 is presented in Figure 4. The zero-point level of the DBS appears right at the detachment threshold and its rotational profile (Figure 3b) clearly reveals the P, Q, and R branches. The sharp peak at 19,602 cm^{-1} (2.4303 eV) should be the Q branch, which is 6 cm^{-1} (0.8 meV) below the detachment threshold at 19,608 cm^{-1} (2.4311 eV) measured from the high-resolution PE spectrum in Figure 2a. Thus, the DBS of indolide is bound by only 6 cm^{-1}, which is the lowest binding energy for a DBS that we have observed. Previously, we reported a DBS binding energy of 8 cm^{-1} in F−$C_6H_4O^-$, whose neutral core has a dipole moment of 2.56 debye.[20]

The photon energies and assignments (*vide infra*) of the seventeen Feshbach resonances are given in Table 2. The photodetachment spectrum is overlaid on the PE spectrum at 2.6206 eV by aligning peak 0 with the 0−0 transition in the PE spectrum (Figure S3). The good agreement between the two different types of spectra confirms that the dipole-bound electron has little effect on the geometry of the neutral indolyl core.

Resonant PE images and spectra are obtained by tuning the detachment laser to the seventeen Feshbach resonances, as shown in Figure 5 (Feshbach resonances 1−8) and Figure 6 (Feshbach resonances 9−17). Resonant PE spectra not only yield rich spectroscopic information about the indolyl radical but are also important to the assignment of the Feshbach resonances, according to the vibrational autodetachment propensity rule ($\Delta v = -1$).[63,64] Compared to the nonresonant PE spectra in Figure 2, one or more vibrational peaks are enhanced (labeled in boldface) in the resonant PE spectra, as well as new peaks (labeled in lowercase letters) that are not observed in the nonresonant PE spectra. The positions of all of the observed vibrational peaks, along with the BEs in both eV and cm^{-1}, shift to the 0_0^0 peak, and their assignments are summarized in Table 1. The detailed assignments of all of the Feshbach resonances and new peaks in the resonant PE spectra will be discussed later.

4. DISCUSSION

4.1. Nonresonant Photoelectron Spectra. In the nonresonant PE spectrum taken at 4.9322 eV (Figure 1), broad vibrational features are resolved for band X in very good agreement with the FC calculations. The (s + d)-wave photoelectron angular distribution displayed in the PE images (Figure 1) agrees with the π HOMO of indolide (Figure S1). Bands A and B at ~3.2 and ~4.3 eV are broad and featureless, suggesting large geometry changes upon photodetachment or strong vibronic couplings.[65] In the nonresonant PE spectra taken at lower photon energies: 2.4346, 2.5300, and 2.6206 eV,
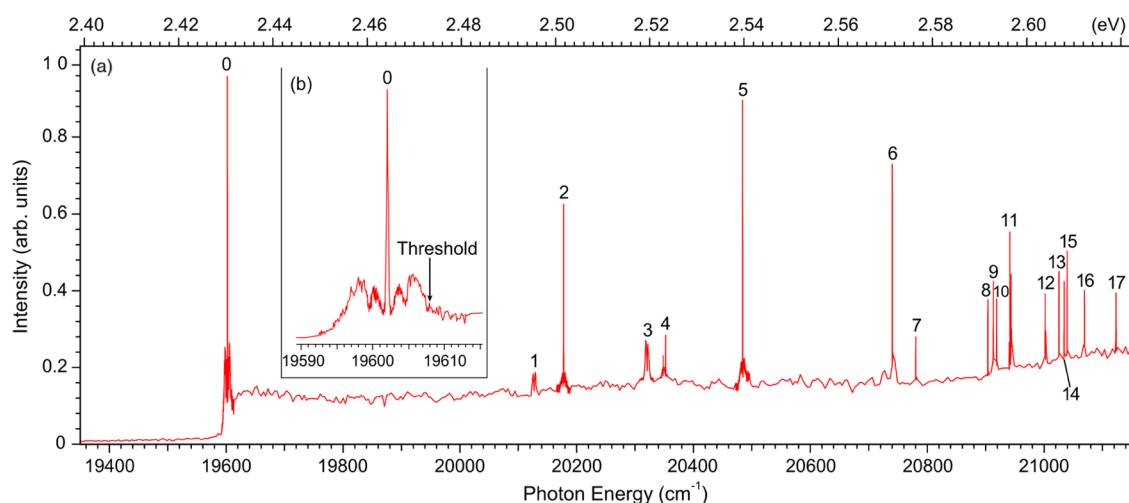
Figure 3. Photodetachment spectrum of indolide by measuring the total electron yield as a function of photon energy. (a) The full spectrum. (b) The inset shows the rotational profile of peak 0. The arrow indicates the detachment threshold at 19,608 cm^{-1} (2.4311 eV).
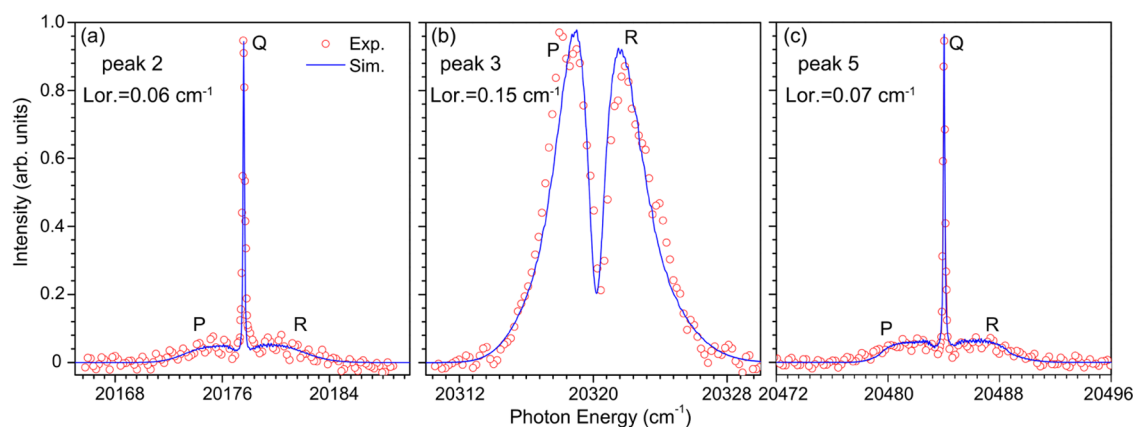

Figure 4. Rotational profiles and simulation for the selected Feshbach resonances. (a) Peak 2, (b) peak 3, and (c) peak 5. Peaks 2 and 5 are c-type transitions, whereas peak 3 is a b-type transition (circles, experimental data; solid line, simulation; T_{rot} = 30 K; Lor.: Lorentz linewidth used for the simulation).

numerous vibrational fine features (A to N) are resolved (Figure 2). The computed FC factors are compared with the high-resolution spectrum in Figure S2. The good agreement between the experiment and the calculated FC factors allows the observed vibrational peaks to be readily assigned, as given in Table 1. Only vibrational modes with A′ symmetry should be active during photodetachment because both the indolide anion and the neutral indolyl final state both have C_s symmetry. Some observed peaks are assigned to more than one vibrational level because several vibrational modes of indolyl have very close computed frequencies (Table S1).

4.2. Vibrational Autodetachment and Resonant PE Spectra. The resonant PE spectra (Figures 5 and 6) contain contributions from two detachment channels: the regular nonresonant photodetachment represented by the continuous signals above the detachment threshold in Figure 3 and the resonantly enhanced autodetachment via vibrational levels (Feshbach resonances) of the DBS. The vibrational structures in the nonresonant PE spectra are determined by the FC principle, as shown by the FC simulations in Figures 1 and S2. Autodetachment from the DBS to final neutral states follows the $\Delta v = -1$ propensity rule,[9,10] i.e., for a single mode excitation, the n-th vibrational level of a given mode ν_x' ($\nu_x'^n$) of the DBS autodetaches to the $(n-1)$-th level of the

corresponding neutral mode (ν_x^{n-1}). The corresponding ν_x^{n-1} vibrational peak will be enhanced relative to that in the nonresonant PE spectrum, giving rise to the mode selectivity and highly non-FC PE spectra.[9] Similarly, for the excitation to a combinational vibrational level ($\nu_x'^m \nu_y'^n \cdots$) of the DBS, the final neutral level from autodetachment can be either $\nu_x^{m-1} \nu_y^n \cdots$ or $\nu_x^m \nu_y^{n-1} \cdots$, according to the $\Delta v = -1$ propensity rule. This propensity of autodetachment is based on the harmonic oscillator parity selection rule, as a result of the fact that the molecular geometry of the DBS is similar to that of the neutral core. Thus, certain vibrational levels are enhanced in the resonant PE spectra, resulting in completely non-FC distributions relative to the nonresonant PE spectra in Figure 2. The vibrational level of the DBS excited in a given resonant PE spectrum is shown in the spectra of Figures 5 and 6, as well as the peak numbers of the corresponding resonant peaks in the photodetachment spectra. The assignments in boldface in Figures 5 and 6 indicate the enhanced vibrational peaks. Based on the vibrational autodetachment propensity rule, in combination with the resonant and nonresonant PE spectra, the comparison between the nonresonant PE spectrum and the photodetachment spectrum (Figure S3), and the calculated vibrational frequencies for indolyl (Table S1), we can assign all

Table 2. Assignments of the Observed Peaks in the Photodetachment Spectra of Indolide, along with Their Wavelength, Photon Energy, and Relative Energy Shift to the Ground Vibrational Level of the DBS

peak	photon energy (eV)	photon energy[a] (cm^{-1})	shift (cm^{-1})	assignment
0	2.4303	19,602	0	DBS ground state
1	2.4952	20,125	523	$36'^1$
2	2.5017	20,178	576	$25'^1$
3	2.5197	20,323	721	$34'^1/39'^126'^1$
4	2.5234	20,352	750	$24'^1/39'^135'^1$
5	2.5397	20,484	882	$22'^1$
6	2.5715	20,740	1138	$18'^1/27'^124'^1/39'^129'^1$
7	2.5765	20,781	1179	$16'^1$
8	2.5918	20,904	1302	$26'^124'^1$
9	2.5929	20,913	1311	$13'^1/25'^124'^1$
10	2.5936	20,919	1317	$13'^1/25'^124'^1$
11	2.5967	20,944	1342	$12'^1/27'^121'^1/$ $39'^117'^1/39'^118'^1$
12	2.6039	21,002	1400	$27'^120'^1$
13	2.6068	21,025	1423	$25'^123'^1$
14	2.6079	21,034	1432	$11'^1/10'^1/39'^134'^126'^1$
15	2.6086	21,040	1438	$34'^2$
16	2.6123	21,069	1467	$9'^1/27'^119'^1/$ $39'^136'^124'^1$
17	2.6189	21,123	1521	$25'^121'^1/24'^2/$ $27'^118'^1/27'^117'^1$

[a]The uncertainty of the peak position is <1 cm^{-1}.

of the Feshbach resonances (Table 2) and the new vibrational peaks observed in the resonant PE spectra (Table 1).

For example, the Feshbach resonance peak 1 is assigned to $36'^1$ (note the prime ' is used to designate DBS vibrational modes), resulting in the enhancement of the 0_0^0 transition in the resonant PE spectrum (Figure 5a), following the $\Delta v = -1$ propensity rule. The sharp tail near threshold (labeled as α in Figure 5a) is due to rotational autodetachment as a result of the extremely low binding energy of the DBS. Similar rotational autodetachment is observed in every resonant PE spectra (Figures 5 and 6), as was also observed in the resonant PE spectra of F-$C_6H_4O^-$ previously,[20] which also possesses a very low DBS binding energy. Resonance 10 is assigned to the combinational mode $(25'^124'^1)$ of the DBS (Figure 6b), where the $24'^1$ vibrational quantum is coupled to the dipole-bound electron, resulting in the enhanced final state B (25^1). Feshbach resonances 8, 9, and 10 are too close to each other and their rotational branches are likely overlapping. They are aligned to peak I (13^1) in the nonresonant PE spectrum (Figure S3). Therefore, the $13'^1$ DBS level is also included in the assignment of the Feshbach resonance 10. The enhancement of peak C (34^1) in Figure 6g indicates that the Feshbach resonance 15 is due to the overtone of mode $34'$ $(34'^2)$. The appearance of the FC-inactive peak g (34^126^1) in Figure 6g is likely due to contribution of the transition in peak 14 (Figure 6f), because Feshbach resonances 13, 14, and 15 are also very close to each other (Figure 3). Due to the high density of vibrational levels, some observed resonances are assigned to
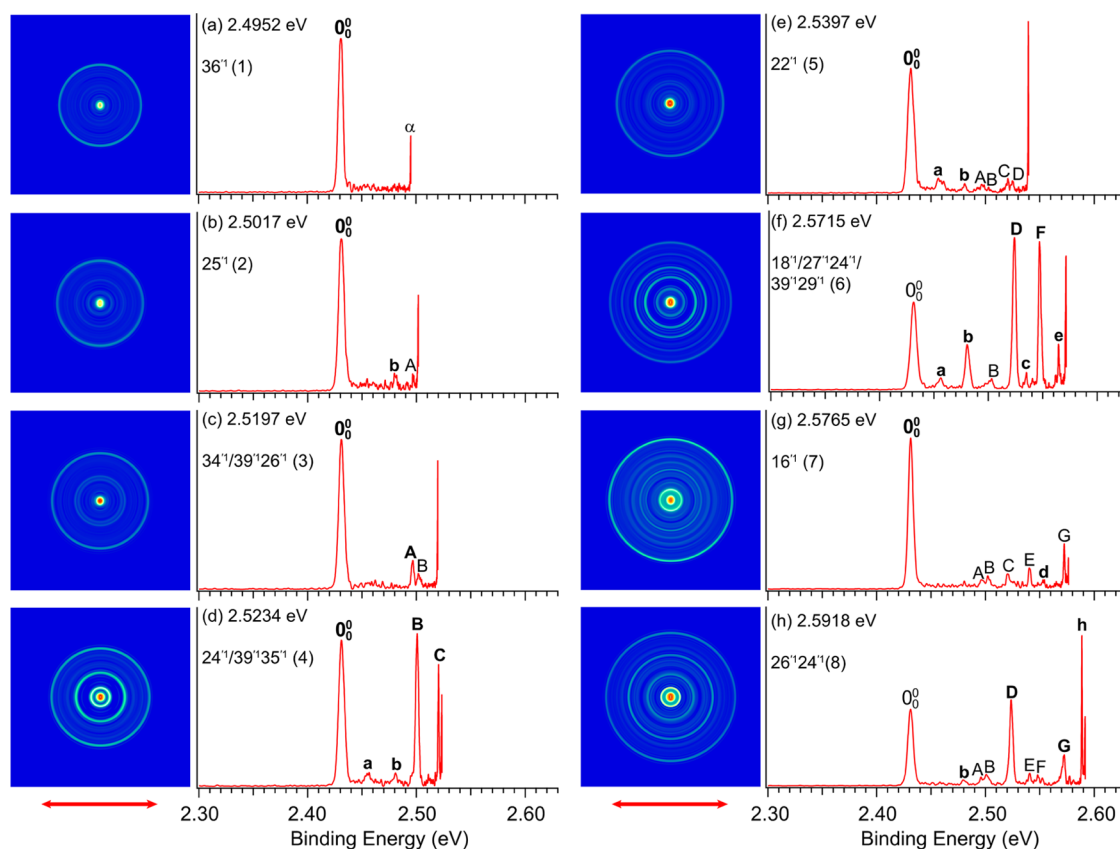

Figure 5. Resonant PE images and spectra of indolide at peaks 1−8 in the PDS (Figure 3) at (a) 2.4952 eV, (b) 2.5017 eV, (c) 2.5197 eV, (d) 2.5234 eV, (e) 2.5397 eV, (f) 2.5715 eV, (g) 2.5765 eV, and (h) 2.5918 eV. The DBS vibrational levels and the corresponding peak number in Figure 3 are given. The autodetachment-enhanced peaks are labeled in boldface. The double arrow below the images indicates the direction of the laser polarization.
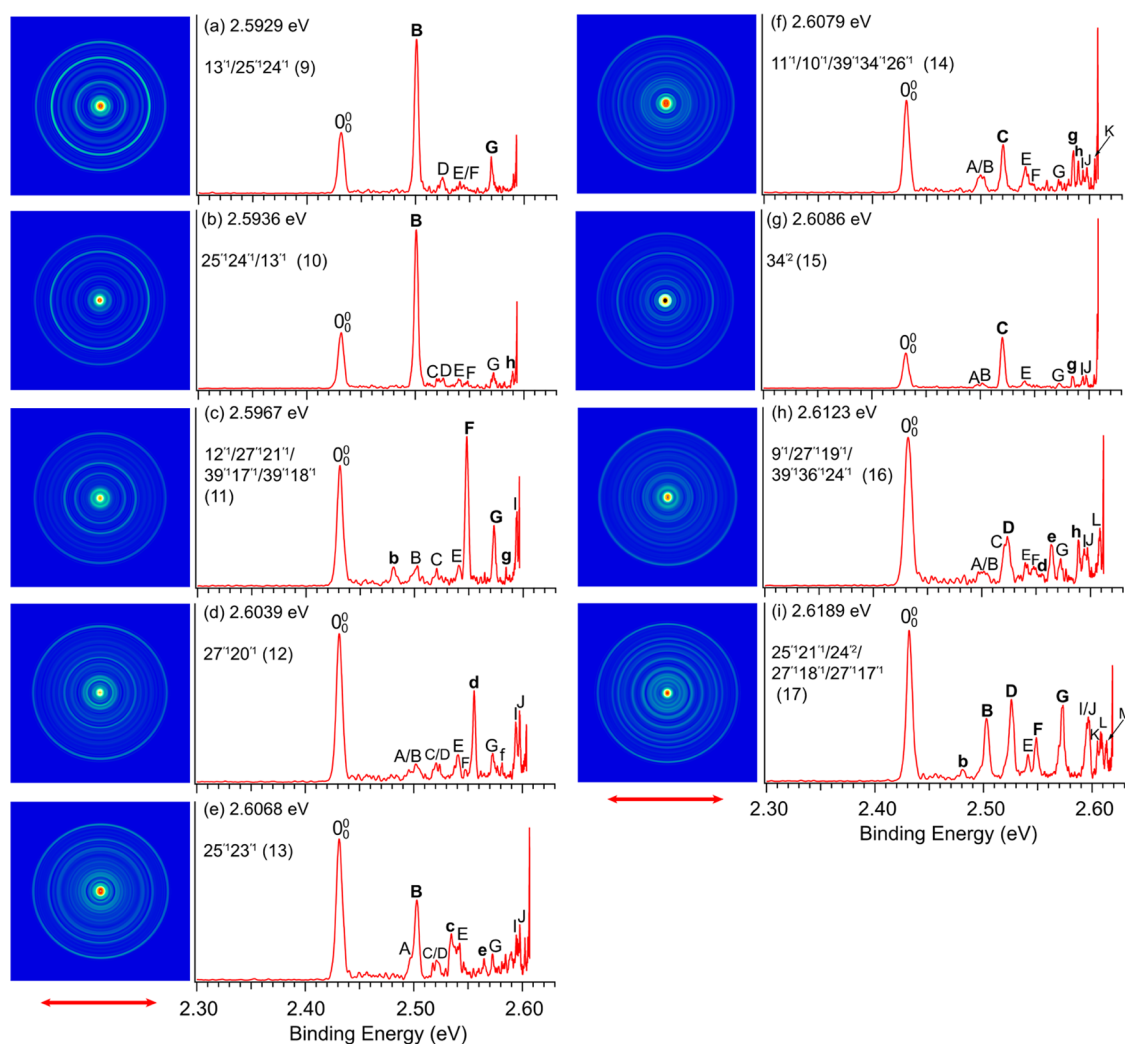
Figure 6. Resonant PE images and spectra of indolide at peaks 9−17 in the PDS (Figure 3) at (a) 2.5929 eV, (b) 2.5936 eV, (c) 2.5967 eV, (d) 2.6039 eV, (e) 2.6068 eV, (f) 2.6079 eV, (g) 2.6086 eV, (h) 2.6123 eV, and (i) 2.6189 eV. The DBS vibrational levels and the corresponding peak number in Figure 3 are given. The autodetachment-enhanced peaks are labeled in boldface. The double arrow below the images indicates the direction of the laser polarization.

multiple vibrational levels of the DBS. Besides the autodetachment-enhanced peaks, some FC-inactive transitions also appear in the resonant PE spectra, especially for low-frequency out-of-plane bending mode, such as peaks a and b in the spectrum at 2.5397 eV (Figure 5e). The appearance of these peaks might be due to the rescattering between the outgoing photoelectron and the neutral core.[66] The assignments of all of the seventeen Feshbach resonances are given in Table 2. A schematic energy level diagram of the Feshbach resonances and the autodetachment processes to the neutral final states is shown in Figure 7. A number of resonant peaks contain overlapping vibrational levels of the DBS. Vibrational frequencies for 25 modes of indolyl were obtained, as summarized in Table 3.

4.3. R2PD PES via the Zero-Point Level of the DBS. As shown in Figures 3b and 8, the rotational profile of the bound zero-point level of the DBS is different from the c-type Feshbach resonances (Figure 4), displaying more structures in the P and R branches. We obtained the R2PD PE spectrum of the zero-point level (Figure S4) and found that the spectrum is dominated by rotational autodetachment (the threshold peak labeled as γ), as a result of rotationally excited states with $E_J >$

6 cm^{-1} in the ground state of the anion (Figure S5), which is also why a broad threshold peak was observed in the previous photodetachment study.[62] Upon careful examination of the lower binding energy part of the R2PD PE spectrum, we also observe the expected sequential two-photon detachment feature at near 0 eV binding energy (peak 0_0^0 in Figure S4b), which contributes less than 1% to the total signal. Weak higher binding energy features are also observed, labeled as $\delta − \iota$ in Figure S4c, due to detachment from rovibrationally excited indolide in its ground electronic state by the second photon as a result of relaxation from the DBS zero-point level upon the absorption of the first photon (II in Figure S5). These peaks can all be assigned to low-lying vibrational excited states of the indolide anion, as shown in Table S5 (the computed vibrational frequencies of the anion are given in Table S2). These observations allowed us to measure vibrational frequencies for several modes of the anion (Table 3). Finally, direct single-photon detachment from the rotationally excited anions ($E_J > 6$ cm^{-1}) is also possible (IV in Figure S5), which should contribute to the threshold feature (γ). Because the rotational autodetachment channel dominates the observed zero-point vibrational band, anions with a rotational energy
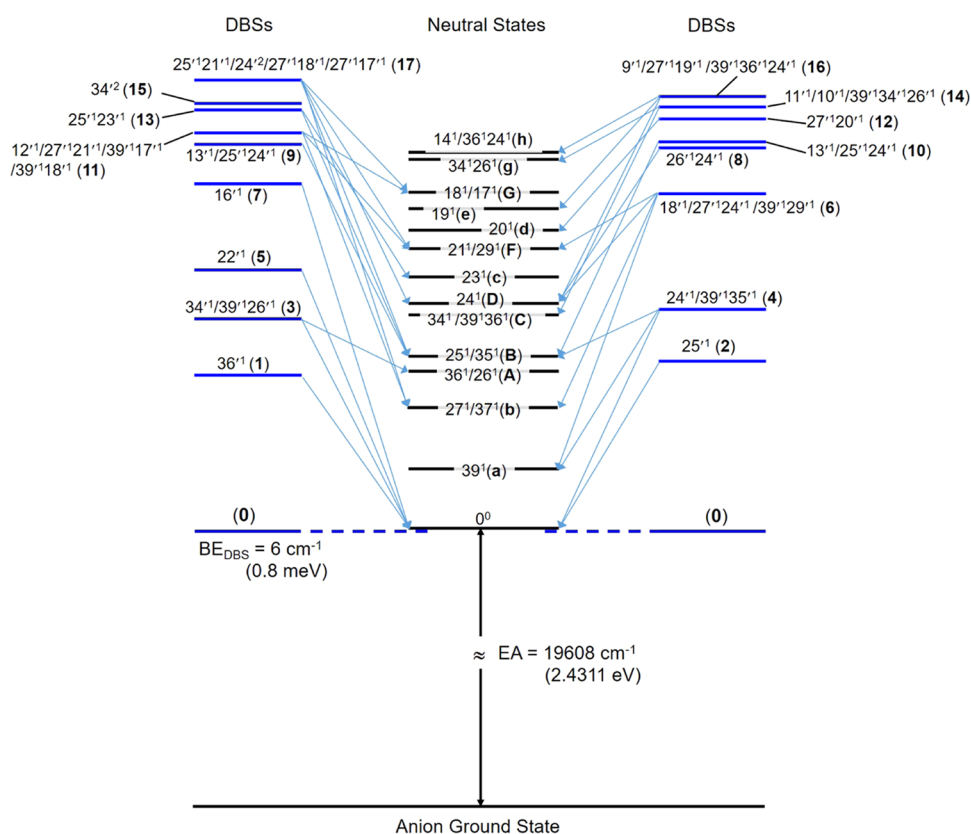
Figure 7. Schematic energy level diagram for autodetachment from seventeen DBS vibrational levels of indolide to the related neutral final states, corresponding to the spectra in Figures 5 and 6.

smaller than 6 cm^{-1} are expected to have little contribution to the total signal. Indeed, the unusual five-peak profile of the zero-point band is qualitatively reproduced by a PGOPHER simulation, if only initial rotational states with $J > \sim 20$ are included (Figure 8).

4.4. Rotational Profile of the Feshbach Resonances and Their Unexpected Long Lifetimes. The most surprising observation is the unprecedented narrow linewidths of the Feshbach resonances. Rotational profiles are resolved for each vibrational resonance at the finest scan step of our dye laser (0.001 nm/step) with distinct P, Q, R branches. Two types of rotational profiles are observed, corresponding to different symmetries of the DBS vibrational levels, i.e., A′ for in-plane modes or A″ for out-of-plane modes, similar to the previous study of the deprotonated uracil anion,[44] but the resonances are much sharper in the current work. Most of the Feshbach resonances correspond to transitions to the FC-active in-plane vibrational modes, which display c-type rotational profiles dominated by a very sharp and intense Q branch, such as resonant peak 2 (ν_{25}', Figure 4a) and peak 5 (ν_{22}', Figure 4c). Resonance peak 1 (ν_{36}') and peak 3 (ν_{34}') correspond to out-of-plane modes, displaying b-type rotational profiles with strong P and R branches, as shown in Figure 4b for peak 3.

The rotational profiles of resonances 2, 3, and 5 are simulated using computed rotational constants and the PGOPHER program,[58] shown as solid lines in Figure 4. The rotational linewidths obtained for resonances 2, 3, and 5 are 0.06, 0.15, and 0.07 cm^{-1}, respectively, and the rotational temperature obtained from the simulation is ~30 K, which is consistent with our previous reports.[44,67] We find that all of the

Feshbach resonances exhibit similar spectral widths, ~0.06 cm^{-1} for the c-type transitions and ~0.15 cm^{-1} for the b-type transitions. The obtained linewidths, in particular, for the c-type transitions, are likely even narrower, limited by the linewidth of our detachment laser (~0.08 cm^{-1}). The measured linewidths allow us to estimate the lower limits of the lifetimes of the Feshbach resonances, ~80 ps for the c-type transitions and ~35 ps for the b-type transitions. Vibrational autodetachment rates for the DBS depend on the coupling between the weakly bound electron and the vibrational motions of the neutral core and exhibit strong mode selectivity as first observed in phenoxide.[43] The lifetime of the DBS has been measured directly using pump−probe experiments for the phenoxide anion, ranging from a few to tens of picoseconds with strong mode dependence.[51] Recently, exceptionally slow autodetachment was observed for the 11′ 1 DBS level of Br−C$_6$H$_6$O$^-$ and was attributed to electron correlation effects.[52] It is quite surprising that all of the Feshbach resonances of indolide exhibit relatively long lifetimes with no strong mode dependence, given the extremely low electron binding energy of only 6 cm^{-1}. This observation suggests that there is very weak coupling between the nearly free dipole-bound electron and the vibrational motions of the indolyl core.

To understand the nature of the DBS, we calculated the low-lying excited electronic states of indolide including diffuse basis sets. Two highly diffuse bound states are found, as shown in Table 4 and Figure 9: a lower π-type DBS with a computed binding energy of 0.17 eV and a slightly higher σ-type DBS with a computed binding energy of 0.16 eV. The orbital of the lower π-DBS is shown to be perpendicular to the permanent dipole direction of the neutral core (Figure 9a and Table S4).

Table 3. Measured Vibrational Frequencies for the Indolyl Radical and the Indolide Anion in This Work, Compared with the Theoretical Values at the DFT/B3LYP/aug-cc-pVTZ Level of Theory

vibrational Mode	symmetry	experimental frequency (cm^{-1})[a]	theoretical frequency (cm^{-1})[b]
ν_9	A'	1469(6)	1465
ν_{10}		1433(7)	1437
ν_{11}		1433(7)	1431
ν_{12}		1345(5)	1346
ν_{13}		1317(5)	1319
ν_{14}		1274(6)	1277
ν_{15}		1210(6)	1208
ν_{16}		1182(10)	1178
ν_{17}		1141(5)	1146
ν_{18}		1141(5)	1139
ν_{19}		1077(5)	1074
ν_{20}		1004(10)	1005
ν_{21}		941(8)	947
ν_{22}		884(8)	881
ν_{23}		839(6)	837
ν_{24}		754(6)	755
ν_{25}		572(8)	575
ν_{26}		526(5)	534
ν_{27}		401(10)	400
ν_{29}	A''	941(8)	944
ν_{34}		720(4)	729
ν_{35}		572(8)	564
ν_{36}		526(5)	532
ν_{37}		401(10)	404
ν_{39}		193(16)	198
ν_{17} (anion)	A'	1136(28)	1153
ν_{18} (anion)		1136(28)	1128
ν_{23} (anion)		839(24)	868
ν_{24} (anion)		751(24)	754
ν_{25} (anion)		592(13)	599
ν_{26} (anion)		527(26)	544
ν_{27} (anion)		402(14)	406

[a]Numbers in the parentheses indicate the experimental uncertainties in the last digit. [b]Scaled by factor 0.98.
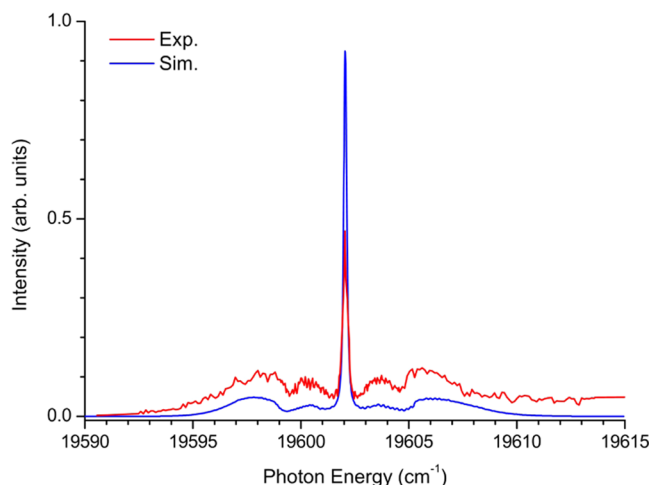

Figure 8. Rotational simulation of the 0−0 transition (red, experimental data; blue, rotational simulation).

The lowest DBS should usually be of σ-symmetry. Apparently, the π-DBS is stabilized by strong polarization interactions with

Table 4. Symmetries, Electronic Configurations, and Calculated Binding Energies (BE) of the Indolide Anion[a]

electronic state	symmetry	dominate electron configuration[b]	BE (eV)[c]
ground state	^{1}A'	···29a'^{2}30a''^{2}31a''^{2}	/
π-DBS	$^{1/3}$A''	···29a'^{2}30a''^{2}31a''^{1}33a'^{1}	0.17
σ-DBS	$^{1/3}$A''	···29a'^{2}30a''^{2}31a''^{1}34a'^{1}	0.16

[a]Calculations were carried out at the TD-DFT/CAM-B3LYP/Def2-TZVPP+4s3p2d1f level of theory under the optimized neutral geometry. [b]The calculated DBS orbitals consist of multiple excitation channels. Only the dominant electronic configuration is shown. [c]The binding energies were calculated by subtracting the vertical excitation energy from the calculated EA (2.28 eV). Note that DFT overestimated the binding energy by ∼0.17 eV in comparison with the experimental data.
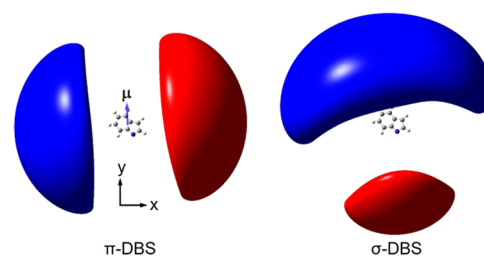

Figure 9. Orbitals of the two lowest energy dipole-bound states of indolide computed at the CAM-B3LYP/Def2-TZVPP+4s3p2d1f level of theory (isovalue = 0.002) (left: π-DBS; right: σ-DBS). The π-DBS is lower in energy.

the delocalized π electrons of the indolyl radical. Indeed, we find that the π-DBS is oriented along the direction of the largest polarizability (Figure 9a and Table S6). This observation is reminiscent of the deprotonated anthrol anion,[47] for which the π-DBS was observed to be lower than the σ-DBS due to strong anisotropic polarization interactions of the π electrons along the aromatic rings. Since the observed binding energy of the DBS in indolide is only 6 cm^{-1} (0.8 meV), the DFT calculation apparently overestimates the DBS binding energy by 0.17 eV, which means the σ-DBS should be unbound by 0.01 eV. Note that the σ-DBS also has a significant π-component because of the substantial polarizability along the permanent dipole direction (Table S6). This result is consistent with the fact that the 2.4 debye dipole moment of indolyl is below the empirical critical dipole moment to support a DBS. Without the anisotropic polarization interactions, no DBS would exist for indolide. Hence, the observed DBS in indolide should be considered as a polarization-assisted π-DBS. The sharp Feshbach resonances suggest weak couplings between the vibrational motions of indolyl and the nearly free dipole-bound electron, resulting in long autodetachment lifetimes for the Feshbach resonances.

5. CONCLUSIONS

In conclusion, we report an investigation of cryogenically cooled indolide anions using high-resolution photoelectron imaging, photodetachment spectroscopy, and resonant photoelectron spectroscopy. The electron affinity of the indolyl radical is accurately measured to be 2.4311 ± 0.0004 eV (19608 ± 3 cm^{-1}). Besides the ground electronic state, the vertical detachment energy for the first two excited electronic states of indolyl are experimentally determined. A dipole-bound state is observed for indolide only 6 cm^{-1} (0.8 meV)

below the detachment. Seventeen sharp vibrational Feshbach resonances are observed. A total of 25 fundamental vibrational frequencies is measured for the indolyl radical, including six Franck–Condon inactive modes. All of the Feshbach resonances are found to have surprisingly narrow linewidths and long autodetachment lifetimes, ~80 ps for c-type transitions, and ~35 ps for b-type transitions, attributed to weak coupling between vibrational motions and the nearly free dipole-bound electron. Calculations suggest that the observed DBS has π-symmetry, which is stabilized by the strong anisotropic polarizability of indolyl. This is the first observation of a polarization-assisted dipole-bound state for a molecule with a dipole moment below 2.5 debye. The stabilization of the DBS by polarization and the observed sharp Feshbach resonances provide a new mechanism to understand the stability and threshold behavior of dipole-bound states.

ASSOCIATED CONTENT

Supporting Information

The Supporting Information is available free of charge at https://pubs.acs.org/doi/10.1021/jacs.3c00246.

> Additional experimental and theoretical results; valence molecular orbitals of the indolide anion; comparison between the experimental nonresonant spectrum at 2.6206 eV (red curve) and the calculated FC factors (blue sticks); R2PD spectrum at 2.4303 eV (19,602 cm^{-1}); calculated vibrational frequencies of indolyl at the DFT/ B3LYP/aug-cc-pVTZ level; symmetries, electronic configurations, and vertical detachment energies (VDEs) of the indolide anion; and assignments of the observed peaks in the R2PD spectrum (PDF)

AUTHOR INFORMATION

Corresponding Author

Lai-Sheng Wang − *Department of Chemistry, Brown University, Providence, Rhode Island 02912, United States;* orcid.org/0000-0003-1816-5738; Email: Lai-Sheng_Wang@brown.edu

Authors

Dao-Fu Yuan − *Department of Chemistry, Brown University, Providence, Rhode Island 02912, United States;* orcid.org/0000-0001-8461-6889

Yuan Liu − *Department of Physics, Massachusetts Institute of Technology, Cambridge, Massachusetts 02139, United States;* orcid.org/0000-0003-1468-942X

Yue-Rou Zhang − *Department of Chemistry, Brown University, Providence, Rhode Island 02912, United States*

Complete contact information is available at:
https://pubs.acs.org/10.1021/jacs.3c00246

Notes

The authors declare no competing financial interest.

ACKNOWLEDGMENTS

REFERENCES

(1) Fermi, E.; Teller, E. The capture of negative mesotrons in matter. *Phys. Rev.* **1947**, *72*, 399−408.

(2) Turner, J. E. Minimum dipole moment required to bind an electron-molecular theorists rediscover phenomenon mentioned in Fermi-Teller paper twenty years earlier. *Am. J. Phys.* **1977**, *45*, 758−766.

(3) Garrett, W. R. Critical binding of an electron to a non-stationary electric dipole. *Chem. Phys. Lett.* **1970**, *5*, 393−397.

(4) Crawford, O. H. Negative ions of polar molecules. *Mol. Phys.* **1971**, *20*, 585−591.

(5) Garrett, W. R. Thermally stable negative ions of polar molecules. *J. Chem. Phys.* **1978**, *69*, No. 2621.

(6) Garrett, W. R. Critical binding and electron scattering by symmetric-top polar molecules. *J. Chem. Phys.* **2014**, *141*, No. 164318.

(7) Slimak, S.; Jordan, K. D. Binding of an electron by a finite fixed dipole. *J. Phys. Chem. Lett.* **2022**, *13*, 10331−10334.

(8) Jordan, K. D.; Wang, F. Theory of dipole-bound anions. *Annu. Rev. Phys. Chem.* **2003**, *54*, 367−396.

(9) Simons, J. Molecular anions. *J. Phys. Chem. A* **2008**, *112*, 6401−6511.

(10) Sommerfeld, T.; Davis, M. C. Excluded-volume descriptors for dipole-bound anions: Amine N⁻ oxides as a test case. *J. Chem. Phys.* **2020**, *152*, No. 054102.

(11) Desfrançois, C.; Abdoul-Carime, H.; Khelifa, N.; Schermann, J-P. From 1/r to 1/r² potentials: electron exchange between Rydberg atoms and polar molecules. *Phys. Rev. Lett.* **1994**, *73*, 2436−2439.

(12) Compton, R. N.; Hammer, N. I. Multiple-Bound Molecular Anions. In *Advances in Gas Phase Ion Chemistry*; Elsevier Science, 2001; Vol. 5, pp 257−305.

(13) Hammer, N. I.; Diri, K.; Jordan, K. D.; Desfrançois, C.; Compton, R. N. Dipole-bound anions of carbonyl, nitrile, and sulfoxide containing molecules. *J. Chem. Phys.* **2003**, *119*, 3650−3660.

(14) Smith, B. H.; Buonaugurio, A.; Chen, J.; Collins, E.; Bowen, K. H.; Compton, R. N.; Sommerfeld, T. Negative ions of p-nitroaniline: Photodetachment, collisions, and ab initio calculations. *J. Chem. Phys.* **2013**, *138*, No. 234304.

(15) Zimmerman, A. H.; Brauman, J. I. Resonances in electron photodetachment cross sections. *J. Chem. Phys.* **1977**, *66*, 5823−5825.

(16) Jackson, R. L.; Hiberty, P. C.; Brauman, J. I. Threshold resonances in the electron photodetachment spectrum of acetaldehyde enolate anion. Evidence for a low-lying dipole-supported state. *J. Chem. Phys.* **1981**, *74*, 3705−3712.

(17) Lykke, K. R.; Mead, R. D.; Lineberger, W. C. Observation of dipole-bound states of negative ions. *Phys. Rev. Lett.* **1984**, *52*, 2221−2224.

(18) Lyykke, K. R.; Neumark, D. M.; Andersen, T.; Trapa, V. J.; Lineberger, W. C. Autodetachment spectroscopy and dynamics of CH₂CN⁻ and CD₂CN⁻. *J. Chem. Phys.* **1987**, *87*, 6842−6853.

(19) Yokoyama, K.; Leach, G. W.; Kim, J. B.; Lineberger, W. C.; Boldyrev, A. I.; Gutowski, M. Autodetachment spectroscopy and dynamics of vibrationally excited dipole-bound states of H₂CCC⁻. *J. Chem. Phys.* **1996**, *105*, 10706−10718.

(20) Qian, C. H.; Zhu, G. Z.; Wang, L. S. Probing the critical dipole moment to support excited dipole-bound states in valence-bound anions. *J. Phys. Chem. Lett.* **2019**, *10*, 6472−6477.

(21) Compton, R. N.; Carman, H. S.; Defrançois, C.; Abdoul-Carmine, H.; Schermann, J. P.; Hendricks, J. H.; Lyapustina, S. A.; Bowen, K. H. On the binding of electrons to nitromethane: Dipole and valence bound anions. *J. Chem. Phys.* **1996**, *105*, 3472−3478.

(22) Mikulski, P.; Klahn, Th.; Krebs, P. Excess electron mobility in low density CH₃CN gas: Short-lived dipole-bound electron ground states as precursors of localized electron states. *Phys. Rev. A* **1997**, *55*, 369−377.

(23) Boudaïffa, B.; Cloutier, P.; Hunting, D.; Huels, M. A.; Sanche, L. Resonant formation of DNA strand breaks by low-energy (3 to 20 eV) electrons. *Science* **2000**, *287*, 1658−1660.

(24) Sommerfeld, T. Coupling between dipole-bound and valence states: The nitromethane anion. *Phys. Chem. Chem. Phys.* **2002**, *4*, 2511–2516.

(25) Fortenberry, R. C.; Crawford, T. D. Theoretical prediction of new dipole-bound singlet states for anions of interstellar interest. *J. Chem. Phys.* **2011**, *134*, No. 154304.

(26) Fortenberry, R. C. Interstellar anions: The role of quantum chemistry. *J. Phys. Chem. A* **2015**, *119*, 9941–9953.

(27) Sarre, P. J. The diffuse interstellar bands: a dipole-bound state hypothesis. *Mon. Not. R. Astron. Soc.* **2000**, *313*, L14–L16.

(28) McCall, B. J.; Oka, T.; Thorburn, J.; Hobbs, L. M.; York, D. G. A critical examination of the I-C₃H₂⁻ spectrum and the diffuse interstellar bands. *Astrophys. J.* **2002**, *567*, L145–L148.

(29) Fortenberry, R. C. Theoretical electronic and rovibrational studies for anions of interest to the DIBs. *Proc. Int. Astron. Union* **2013**, *9*, 344–348.

(30) Guthe, F.; Tulej, M.; Pachkov, M. V.; Maier, J. P. Photodetachment spectrum of I-C₃H₂⁻: the role of dipole-bound states for electron attachment in interstellar clouds. *Astrophys. J.* **2001**, *555*, 466–471.

(31) Laws, B. A.; Levey, Z. D.; Schmidt, T. W.; Gibson, S. T. Velocity map imaging spectroscopy of the dipole-bound state of CH₂CN⁻: implications for the diffuse interstellar bands. *J. Am. Chem. Soc.* **2021**, *143*, 18684–18692.

(32) Dessent, C. E. H.; Kim, J.; Johnson, M. A. Photochemistry of halide ion-molecule clusters: dipole-bound excited states and the case for asymmetric solvation. *Acc. Chem. Res.* **1998**, *31*, 527–534.

(33) Suess, L.; Liu, Y.; Parthasarathy, R.; Dunning, F. B. Dipole-bound negative ions: Collisional destruction and blackbody-radiation-induced photodetachment. *J. Chem. Phys.* **2003**, *119*, 12890–12894.

(34) Dao, D. B.; Mabbs, R. The effect of the dipole bound state on AgF⁻ vibrationally resolved photodetachment cross sections and photoelectron angular distributions. *J. Chem. Phys.* **2014**, *141*, No. 154304.

(35) Mascaritolo, K. J.; Gardner, A. M.; Heaven, M. C. Autodetachment spectroscopy of the aluminum oxide anion dipole bound state. *J. Chem. Phys.* **2015**, *143*, No. 114311.

(36) Ciborowski, S. M.; Liu, G.; Graham, J. D.; Buytendyk, A. M.; Bowen, K. H. Dipole-bound anions: formed by Rydberg electron transfer (RET) and studied by velocity map imaging-anion photoelectron spectroscopy (VMI-aPES). *Eur. Phys. J. D* **2018**, *72*, No. 139.

(37) Kunin, A.; Neumark, D. M. Time-resolved radiation chemistry: femtosecond photoelectron spectroscopy of electron attachment and photodissociation dynamics in iodide-nucleobase clusters. *Phys. Chem. Chem. Phys.* **2019**, *21*, 7239–7255.

(38) Castellani, M. E.; Anstöter, C. S.; Verlet, J. R. R. On the stability of a dipole-bound state in the presence of a molecule. *Phys. Chem. Chem. Phys.* **2019**, *21*, 24286–24290.

(39) Lu, Y.; Tang, R.; Ning, C. Observation of an excited dipole-bound state in a diatomic anion. *J. Phys. Chem. Lett.* **2021**, *12*, 5897–5902.

(40) Simpson, M.; Nötzold, M.; Michaelsen, T.; Wild, R.; Gianturco, F. A.; Wester, R. Influence of a supercritical electric dipole moment on the photodetachment of C₃N⁻. *Phys. Rev. Lett.* **2021**, *127*, No. 043001.

(41) Wang, X. B.; Wang, L. S. Development of a low-temperature photoelectron spectroscopy instrument using an electrospray ion source and a cryogenically controlled ion trap. *Rev. Sci. Instrum.* **2008**, *79*, No. 073108.

(42) Wang, L. S. Electrospray photoelectron spectroscopy: From multiply-charged anions to ultracold anions. *J. Chem. Phys.* **2015**, *143*, No. 040901.

(43) Liu, H. T.; Ning, C. G.; Huang, D. L.; Dau, P. D.; Wang, L. S. Observation of mode-specific vibrational autodetachment from dipole-bound states of cold anions. *Angew. Chem., Int. Ed.* **2013**, *52*, 8976–8979.

(44) Liu, H. T.; Ning, C. G.; Huang, D. L.; Wang, L. S. Vibrational spectroscopy of the dehydrogenated uracil radical via autodetachment of dipole-bound excited states of cold anions. *Angew. Chem., Int. Ed.* **2014**, *53*, 2464–2468.

(45) Zhu, G. Z.; Huang, D. H.; Wang, L. S. Conformation-selective resonant photoelectron imaging from dipole-bound states of cold 3-hydroxyphenoxide. *J. Chem. Phys.* **2017**, *147*, No. 013910.

(46) Zhu, G. Z.; Wang, L. S. High-resolution photoelectron imaging and resonant photoelectron spectroscopy via noncovalent-bound excited states of cryogenically-cooled anions. *Chem. Sci.* **2019**, *10*, 9409–9423.

(47) Yuan, D. F.; Liu, Y.; Qian, C. H.; Zhang, Y. R.; Rubenstein, B. M.; Wang, L. S. Observation of a π-type dipole-bound state in m olecular anions. *Phys. Rev. Lett.* **2020**, *125*, No. 073003.

(48) Qian, C. H.; Zhang, Y. R.; Yuan, D. F.; Wang, L. S. Photodetachment spectroscopy and resonant photoelectron imaging of cryogenically cooled 1-pyrenolate. *J. Chem. Phys.* **2021**, *154*, No. 094308.

(49) Zhang, Y. R.; Yuan, D. F.; Wang, L. S. Observation of core-excited dipole-bound states. *J. Phys. Chem. Lett.* **2022**, *13*, 2124–2129.

(50) Yuan, D. F.; Zhang, Y. R.; Wang, L. S. Dipole-bound state, photodetachment spectroscopy, and resonant photoelectron imaging of cryogenically-cooled 2-cyanopyrrolide. *J. Phys. Chem. A* **2022**, *126*, 6416–6428.

(51) Kang, D. H.; An, S.; Kim, S. K. Real-time autodetachment dynamics of vibrational Feshbach resonances in a dipole-bound state. *Phys. Rev. Lett.* **2020**, *125*, No. 093001.

(52) Kang, D. H.; Kim, J.; Kim, S. K. Dynamic role of the correlation effect revealed in the exceptionally slow autodetachment rates of the vibrational Feshbach resonances in the dipole-bound state. *Chem. Sci.* **2022**, *13*, 2714–2720.

(53) Kang, D. H.; Kim, J.; Eun, H. J.; Kim, S. K. State-specific chemical dynamics of the nonvalence bound state of the molecular anions. *Acc. Chem. Res.* **2022**, *55*, 3032–3042.

(54) Garcia, G. A.; Nahon, L.; Powis, I. Two-dimensional charged particle image inversion using a polar basis function expansion. *Rev. Sci. Instrum.* **2004**, *75*, 4989–4996.

(55) Dribinski, V.; Ossadtchi, A.; Mandelshtam, V. A.; Reisler, H. Reconstruction of Abel-transformable images: The Gaussian basis-set expansion Abel transform method. *Rev. Sci. Instrum.* **2002**, *73*, 2634–2642.

(56) Pugliesi, I.; Müller-Dethlefs, K. The use of multidimensional Franck-Condon simulations to assess model chemistries: A case study on phenol. *J. Phys. Chem. A* **2006**, *110*, 4657–4667.

(57) Frisch, M. J.; Trucks, G. W.; Schlegel, H. B.; Scuseria, G. E.; Robb, M. A.; Cheeseman, J. R.; Scalmani, G.; Barone, V.; Petersson, G. A.; Nakatsuji, H.; Li, X.; Caricato, M.; Marenich, A.; Bloino, J.; Janesko, B. G.; Gomperts, R.; Mennucci, B.; Hratchian, H. P.; Ortiz, J. V.; Izmaylov, A. F.; Sonnenberg, J. L.; Williams-Young, D.; Ding, F.; Lipparini, F.; Egidi, F.; Goings, J.; Peng, B.; Petrone, A.; Henderson, T.; Ranasinghe, D.; Zakrzewski, V. G.; Gao, J.; Rega, N.; Zheng, G.; Liang, W.; Hada, M.; Ehara, M.; Toyota, K.; Fukuda, R.; Hasegawa, J.; Ishida, M.; Nakajima, T.; Honda, Y.; Kitao, O.; Nakai, H.; Vreven, T.; Throssell, K.; Montgomery, J. A., Jr; Peralta, J. E.; Ogliaro, F.; Bearpark, M.; Heyd, J. J.; Brothers, E.; Kudin, K. N.; Staroverov, V. N.; Keith, T.; Kobayashi, R.; Normand, J.; Raghavachari, K.; Rendell, A.; Burant, J. C.; Iyengar, S. S.; Tomasi, J.; Cossi, M.; Millam, J. M.; Klene, M.; Adamo, C.; Cammi, R.; Ochterski, J. W.; Martin, R. L.; Morokuma, K.; Farkas, O.; Foresman, J. B.; Fox, D. J. *Gaussian 09*, Revision D.01; Gaussian, Inc.: Wallingford CT, 2016.

(58) Western, C. M. PGOPHER: A Program for Simulating Rotational Structure *University of Bristol*, 2022, http://pgopher.chm.bris.ac.uk.

(59) Herzberg, G. *Molecular Spectra and Molecular Structure. III. Electronic Spectra and Electronic Structure of Polyatomic Molecules*; Van Nostrand Reinhold: New York, 1966.

(60) Nelson, D. J.; Oliveira, A. M.; Lineberger, W. C. Anion photoelectron spectroscopy of deprotonated indole and indoline. *J. Chem. Phys.* **2018**, *148*, No. 064307.

(61) Parkes, M. A.; Crellin, J.; Henley, A.; Fielding, H. H. A photoelectron imaging and quantum chemistry study of the

deprotonated indole anion. *Phys. Chem. Chem. Phys.* **2018**, *20*, 15543−15549.

(62) Noble, J. A.; Marceca, E.; Dedonder, C.; Jouvet, C. Influence of the N atom and its position on electron photodetachment of deprotonated indole and azaindole. *Phys. Chem. Chem. Phys.* **2020**, *22*, 27290−27299.

(63) Berry, R. S. Ionization of molecules at low energies. *J. Chem. Phys.* **1966**, *45*, 1228−1245.

(64) Simons, J. Propensity rules for vibrational-induced electron detachment of anions. *J. Am. Chem. Soc.* **1981**, *103*, 3971−3976.

(65) Zhang, Y. R.; Yuan, D. F.; Wang, L. S. Probing the electronic structure and spectroscopy of pyrrolyl and imidazolyl radicals using high-resolution photoelectron imaging of cryogenically cooled anions. *Phys. Chem. Chem. Phys.* **2022**, *24*, 6505−6514.

(66) Huang, D. L.; Liu, H. T.; Ning, C. G.; Dau, P. D.; Wang, L. S. Resonant photoelectron imaging of deprotonated uracil anion via vibrational levels of a dipole-bound excited state. *Chem. Phys.* **2017**, *482*, 374−383.

(67) Zhu, G. Z.; Liu, Y.; Wang, L. S. Observation of excited quadrupole-bound states in cold anions. *Phys. Rev. Lett.* **2017**, *119*, No. 023002.

▥ Recommended by ACS